

Relative ^{11}C -PiB Delivery as a Proxy of Relative CBF: Quantitative Evaluation Using Single-Session ^{15}O -Water and ^{11}C -PiB PET

Yin J. Chen¹, Bedda L. Rosario², Wenzhu Mowrey², Charles M. Laymon¹, Xueling Lu¹, Oscar L. Lopez³, William E. Klunk⁴, Brian J. Lopresti¹, Chester A. Mathis¹, and Julie C. Price¹

¹Department of Radiology, University of Pittsburgh School of Medicine, Pittsburgh, Pennsylvania; ²Department of Biostatistics, University of Pittsburgh School of Medicine, Pittsburgh, Pennsylvania; ³Department of Neurology, University of Pittsburgh School of Medicine, Pittsburgh, Pennsylvania; and ⁴Department of Psychiatry, University of Pittsburgh School of Medicine, Pittsburgh, Pennsylvania

The primary goal of this study was to assess the suitability of ^{11}C -Pittsburgh compound B (^{11}C -PiB) blood-brain barrier delivery (K_1) and relative delivery (R_f) parameters as surrogate indices of cerebral blood flow (CBF), with a secondary goal of directly examining the extent to which simplified uptake measures of ^{11}C -PiB retention (amyloid- β load) may be influenced by CBF, in a cohort of controls and patients with mild cognitive impairment (MCI) and Alzheimer disease (AD). **Methods:** Nineteen participants (6 controls, 5 AD, 8 MCI) underwent MR imaging, ^{15}O -water PET, and ^{11}C -PiB PET in a single session. Fourteen regions of interest (including cerebellar reference region) were defined on MR imaging and applied to dynamic coregistered PET to generate time-activity curves. Multiple analysis approaches provided regional ^{15}O -water and ^{11}C -PiB measures of delivery and ^{11}C -PiB retention that included compartmental modeling distribution volume ratio (DVR), arterial- and reference-based Logan DVR, simplified reference tissue modeling 2 (SRTM2) DVR, and standardized uptake value ratios. Spearman correlation was performed among delivery measures (i.e., ^{15}O -water K_1 and ^{11}C -PiB K_1 , relative K_1 normalized to cerebellum [Rel- $K_{1\text{-Water}}$ and Rel- $K_{1\text{-PiB}}$], and ^{11}C -PiB SRTM2- R_f) and between delivery measures and ^{11}C -PiB retention, using the Bonferroni method for multiple-comparison correction. **Results:** Primary analysis showed positive correlations ($\rho \approx 0.2\text{--}0.5$) between ^{15}O -water K_1 and ^{11}C -PiB K_1 that did not survive Bonferroni adjustment. Significant positive correlations were found between Rel- $K_{1\text{-Water}}$ and Rel- $K_{1\text{-PiB}}$ and between Rel- $K_{1\text{-Water}}$ and ^{11}C -PiB SRTM2- R_f ($\rho \approx 0.5\text{--}0.8$, $P < 0.0036$) across primary cortical regions. Secondary analysis showed few significant correlations between ^{11}C -PiB retention and relative ^{11}C -PiB delivery measures (but not ^{15}O -water delivery measures) in primary cortical areas that arose only after accounting for cerebrospinal fluid dilution. **Conclusion:** ^{11}C -PiB SRTM2- R_f is highly correlated with regional relative CBF, as measured by ^{15}O -water K_1 normalized to cerebellum, and cross-sectional ^{11}C -PiB retention did not strongly depend on CBF across primary cortical regions. These results provide further support for potential dual-imaging assessments of regional brain status (i.e., amyloid- β load and relative CBF) through dynamic ^{11}C -PiB imaging.

Key Words: amyloid; blood flow; PiB PET; Alzheimer's disease; kinetic modeling

J Nucl Med 2015; 56:1199–1205
DOI: 10.2967/jnumed.114.152405

The development of β -amyloid (A β) plaque imaging agents, such as ^{11}C -Pittsburgh compound B (^{11}C -PiB), for PET has enabled measurement of A β deposition in living humans (1–3). These studies demonstrated 2-fold-greater ^{11}C -PiB cortical retention in Alzheimer disease (AD) patients (relative to cognitively normal controls), evidence of A β deposition in 50%–70% of patients with mild cognitive impairment (MCI) (4,5), and elevated ^{11}C -PiB retention in 10%–30% of elderly controls (average age, 64–74 y) (2,4,6–10).

Despite a multitude of ^{11}C -PiB studies, few were fully quantitative kinetic modeling studies (11–13) because this involves invasive arterial blood sampling and long scan duration that can be burdensome for subjects, and simplified PET methodologies were found to provide assessments of A β load that are consistent with quantitative outcomes (14,15).

Fully quantitative PET studies provide important information needed to evaluate radiotracer kinetics (e.g., blood-brain barrier radioligand delivery [K_1], specific binding [k_3]) and strengths and limitations of more feasible semiquantitative methods (e.g., reference Logan, simplified reference tissue model [SRTM], multilinear reference tissue model [MRTM], and standardized uptake value tissue ratios [SUVRs]) (14–18).

Meyer et al. reported on dual-biomarker imaging with ^{11}C -PiB using the 2-step SRTM method (SRTM2) to assess both A β plaque load and regional relative radioligand delivery R_f , showing good correlation between ^{11}C -PiB SRTM2- R_f and ^{18}F -FDG SUVR (40–60 min after injection) (19). Meyer et al. concluded that ^{11}C -PiB can provide information on not only A β load but also neuronal activity and neurodegeneration through SRTM2- R_f .

Van Berckel et al. recently examined longitudinal changes in ^{11}C -PiB retention using voxel-based parametric approaches, ranging from SUVR to a voxel-level reference tissue analog of SRTM2 (RPM2) and found sensitivity of longitudinal changes in ^{11}C -PiB SUVR to changes in flow (20).

Received Nov. 28, 2014; revision accepted May 24, 2015.
For correspondence or reprints contact: Julie C. Price, University of Pittsburgh School of Medicine, PET Facility, PUH B-938, 200 Lothrop St., Pittsburgh, PA 15213.
E-mail: pricejc@upmc.edu
Published online Jun. 4, 2015.
COPYRIGHT © 2015 by the Society of Nuclear Medicine and Molecular Imaging, Inc.

The primary goal of this study was to clarify, through quantitative evaluation of ^{15}O -water and ^{11}C -PiB delivery parameters, the extent to which ^{11}C -PiB SRTM2- R_I can be a robust surrogate index of relative cerebral blood flow (CBF). Secondly, regional relationships between ^{15}O -water and ^{11}C -PiB delivery parameters and ^{11}C -PiB retention were examined to further clarify independence between these measures, on a cross-sectional basis, particularly for simplified retention measures.

MATERIALS AND METHODS

Human Subjects

Nineteen subjects (6 controls, 8 MCI, 5 AD) were recruited, as previously described (13,15). Subject characteristics are shown in Table 1. This study was approved by the local Institutional Review Board, and informed consent was obtained from all subjects or their caregivers. Some ^{11}C -PiB PET results were previously published (8,13,15,17) with exceptions noted below. The basic imaging methodology is described below, with further details in earlier publications (13,15,21).

Imaging

MR imaging (spoiled-gradient recalled sequence) was performed on a 1.5-T Signa (GE Healthcare) scanner for region-of-interest (ROI) definition and determination of atrophy-related cerebrospinal fluid (CSF) dilution. A Siemens/CTI ECAT-HR+ PET scanner was used with a Neuro-insert (CTI PET Systems), as previously reported (13). PET corrections included scanner normalization, deadtime, attenuation, scatter, random coincidences, and radioactive decay. PET data were reconstructed by filtered backprojection (direct Fourier method; final spatial resolution, ~ 6 mm).

^{15}O -water was synthesized using a mixed gas flow system, trapped in saline solution (5–7 mL), and administered as a rapid bolus (444 MBq) using an automated injector system, with simultaneous initiation of a 3-min 20-frame dynamic acquisition (10×3 , 3×10 , 4×15 , and 3×20 s). Ten minutes after ^{15}O -water imaging, a transmission scan ($^{68}\text{Ge}/^{68}\text{Ga}$ rods) was acquired. ^{11}C -PiB, synthesized as previously described (13), was administered as a slow 20-s bolus (~ 500 MBq, 50 GBq/ μmol) with simultaneous start of a 90-min 34-frame dynamic acquisition (4×15 , 8×30 , 9×60 , 2×180 , 8×300 , and 3×600 s).

Plasma input functions were determined using dynamic arterial blood sampling (radial artery) performed over 3.5 min for ^{15}O -water using a Siemens Liquid Activity Monitoring System and over 90 min for ^{11}C -PiB by manual collection of 35 samples (0.5 mL), with 20 collected within 2 min and 5–6 additional samples (2–3 mL) collected over the study, to measure radiolabeled metabolites.

Image Processing and ROI Definition

The ^{15}O -water and ^{11}C -PiB PET data were separately coregistered to MR images using automated registration methods (22,23), as de-

scribed previously (15,24). The ^{15}O -water and ^{11}C -PiB data were integrated over the initial 3 and 15 min, respectively. Each integrated PET image was aligned to a MR image, and the MR image was resliced to match PET space ($128 \times 128 \times 63$; pixel size, $2.06 \times 2.06 \times 2.43$ mm).

ROIs were manually defined on coregistered MR images using criteria that resulted in high rater reliability (24). ROIs included anterior cingulate gyrus (ACG), anterior ventral striatum (AVS), cerebellum (CER), frontal cortex (FRC), lateral temporal cortex (LTC), mesial temporal cortex (MTC), occipital cortex (OCC), occipital pole (OCP), parietal cortex (PAR), pons (PON), precuneus (PRC), sensory-motor cortex (SMC), subcortical white matter (SWM), and thalamus (THL). A global cortical region (CTX5) was defined as the voxel-weighted average of ACG, FRC, LTC, PAR, and PRC (primary cortical regions). ROIs were applied to sample dynamic PET data and generate regional time-activity curves. CER was used as the reference region to approximate the kinetics of nondisplaceable (ND) uptake and defined to minimize white matter uptake and spillover effects from OCC. For ^{15}O -water, CER was also used as a reference, because it is less prone to age-related atrophy and changes in CBF (25).

Data Analysis

^{15}O -water data were analyzed using a 1-tissue compartment model with iterative curve-fitting to estimate ^{15}O -water K_1 ($\text{mL}\cdot\text{cm}^{-3}\cdot\text{min}^{-1}$) and brain efflux k_2 (min^{-1}), while accounting for input function timing delays, as previously described (21). In this work, $K_{1\text{-Water}}$ was used as a direct index of CBF (i.e., $K_{1\text{-Water}} = F \times E = F \times [1 - e^{-PSF}]$, where E = extraction fraction, F = CBF, and PS = permeability surface area product), although limitations in ^{15}O -water single-pass extraction ($\sim 90\%$) are well known (26). Relative $K_{1\text{-Water}}$ ($\text{Rel-}K_{1\text{-Water}}$) was computed regionally as the $K_{1\text{-Water-ROI}}/K_{1\text{-Water-CER}}$ ratio.

Multiple modeling approaches were used to analyze ^{11}C -PiB. As previously described (13,15), a 2-tissue, 4-parameter compartment model (2T-4k), Logan analysis (using arterial [ART90] or cerebellar reference [CER90] [90 is the total length of the scan, 90 min] data as input), and SRTM2 were applied (15). SRTM2 was applied by constraining k_2' (reference tissue clearance rate) to the mean of the k_2' values initially determined using SRTM across all ROIs except CER for each subject.

For the primary analysis, ^{11}C -PiB delivery measures were obtained from compartmental modeling, including $K_{1\text{-PiB}}$ and relative $K_{1\text{-PiB}}$ ($\text{Rel-}K_{1\text{-PiB}} = K_{1\text{-PiB-ROI}}/K_{1\text{-PiB-CER}}$ ratio), and SRTM2- R_I (representing $K_{1\text{-PiB-ROI}}/K_{1\text{-PiB-CER}}$ ratio). For the secondary analysis, ^{11}C -PiB retention measures were based on 2T-4k distribution volumes (i.e., $V_T = K_1/k_2[1 + k_3/k_4]$) used to compute distribution volume ratios (DVR), that is, $\text{DVR} = V_{T\text{-ROI}}/V_{T\text{-CER}} = \text{BP}_{ND} + 1$, where BP_{ND} (binding potential nondisplaceable) is directly related to density of available binding sites (B_{avail}) and radioligand affinity (27). DVR was computed using the 2T-4k model, Logan analysis, and SRTM2

TABLE 1
Subject Characteristics

Characteristic	Controls ($n = 6$)	MCI ($n = 8$)	AD ($n = 5$)	Group comparison (Kruskal-Wallis P)
Sex				–
Male	1	6	4	
Female	5	2	1	
Age (y)	62.8 \pm 11.8	69.0 \pm 10.5	67.0 \pm 9.0	0.529
MMSE	28.5 \pm 1.4	27.8 \pm 1.0	24.0 \pm 3.4	0.010
Education (y)	14.2 \pm 2.4	17.5 \pm 3.4	17.4 \pm 3.6	0.137

TABLE 2
Delivery Parameters

Parameter	$K_{1\text{-Water}}^*$	$K_{1\text{-PiB}}^*$	Rel- $K_{1\text{-Water}}^\dagger$	Rel- $K_{1\text{-PiB}}^\dagger$	SRTM2- R_7^\dagger
ACG	0.520 ± 0.096	0.280 ± 0.045	0.994 ± 0.14	0.920 ± 0.11	0.911 ± 0.096
FRC	0.455 ± 0.079	0.271 ± 0.046	0.868 ± 0.096	0.886 ± 0.080	0.869 ± 0.071
LTC	0.408 ± 0.079	0.251 ± 0.045	0.780 ± 0.10	0.821 ± 0.078	0.835 ± 0.072
PAR	0.444 ± 0.088	0.277 ± 0.049	0.850 ± 0.13	0.909 ± 0.098	0.888 ± 0.079
PRC	0.531 ± 0.010	0.316 ± 0.058	1.013 ± 0.13	1.035 ± 0.11	0.988 ± 0.089
CTX5	0.467 ± 0.083	0.278 ± 0.048	0.891 ± 0.11	0.912 ± 0.083	0.894 ± 0.073
MTC	0.446 ± 0.074	0.199 ± 0.028	0.855 ± 0.098	0.660 ± 0.089	0.713 ± 0.069
OCC	0.537 ± 0.11	0.335 ± 0.061	1.029 ± 0.19	1.097 ± 0.10	1.028 ± 0.091
AVS	0.467 ± 0.093	0.287 ± 0.052	0.887 ± 0.081	0.940 ± 0.097	0.915 ± 0.074
SWM	0.180 ± 0.032	0.098 ± 0.024	0.350 ± 0.087	0.319 ± 0.060	0.367 ± 0.059
PON	0.402 ± 0.081	0.238 ± 0.042	0.764 ± 0.076	0.777 ± 0.061	0.796 ± 0.059

*In mL·cm⁻³·min⁻¹.

†Unitless.

Parameters adjusted for CSF dilution.

(i.e., $BP_{ND} + I$). ¹¹C-PiB retention was also measured using SUVRs measured over 50–70 min after injection (SUVR70), with $SUVR_{ROI} = SUVR_{ROI}/SUVR_{CER}$ (15).

The delivery and ¹¹C-PiB retention measures were adjusted for dilutional effects of expanded CSF spaces, using an MR imaging-guided approach routinely used at our site (28,29). Most processing and analysis software was developed and validated in-house, except for SRTM/SRTM2 analyses performed in PMOD 3.204 (PMOD Technologies Ltd.). Parametric images were generated for Rel- $K_{1\text{-Water}}$ using a voxel-based in-house implementation of the 1-tissue model, and SRTM- R_7 and DVR images were generated using PMOD.

Statistical Methods

Descriptive statistics included mean ± SD or counts, as appropriate. Relative SD (RSD, expressed as percentages) was calculated for delivery measures to assess differences in intersubject variability. Group differences in subject characteristics were determined using the Kruskal–Wallis test, with the Mann–Whitney U test for post hoc comparisons. The Bonferroni method was used for multiple-comparison correction.

Relationships between outcome measures were examined using Spearman correlation, on a region-by-region basis across all subjects. The primary correlations were between measures of CBF and ¹¹C-PiB delivery ($K_{1\text{-Water}}$ vs. $K_{1\text{-PiB}}$, Rel- $K_{1\text{-Water}}$ vs. Rel- $K_{1\text{-PiB}}$, Rel- $K_{1\text{-Water}}$ vs. ¹¹C-PiB SRTM2- R_7 , and Rel- $K_{1\text{-PiB}}$ vs. ¹¹C-PiB SRTM2- R_7). Secondary correlations were between delivery parameters ($K_{1\text{-Water}}$, Rel- $K_{1\text{-Water}}$, $K_{1\text{-PiB}}$, and Rel- $K_{1\text{-PiB}}$) and ¹¹C-PiB retention (2T-4k-DVR, ART90-DVR, CER90-DVR, SRTM2-DVR, and SUVR70). Correlations were performed with and without CSF dilution adjustment. All analyses were 2-sided and underwent Bonferroni adjustment where appropriate. Statistical analyses were performed using SPSS 20.0.0 (IBM Corp.).

RESULTS

Subjects and CSF Correction

Neither age nor education was significantly different across subject groups (Table 1). Mini Mental State Examination (MMSE) scores were significantly different ($P = 0.010$). Post hoc analysis

showed higher MMSE for controls than AD ($P = 0.009$) and higher MMSE for MCI than AD ($P = 0.011$), which survived Bonferroni adjustment. CSF dilution factors (Supplemental Table 1; supplemental materials are available at <http://jnm.nmjournal.org>) were not significantly different across subject groups, after Bonferroni adjustment, as previously reported (15).

Delivery Parameters

Table 2 shows mean regional delivery parameters. On average, $K_{1\text{-PiB}}$ was 40%–50% lower than $K_{1\text{-Water}}$ for most ROIs. In contrast, average relative ¹⁵O-water and ¹¹C-PiB delivery parameters were more similar. Supplemental Figure 1 plots $K_{1\text{-Water}}$ and $K_{1\text{-PiB}}$ for primary cortical ROIs, CER, and PON grouped by diagnosis.

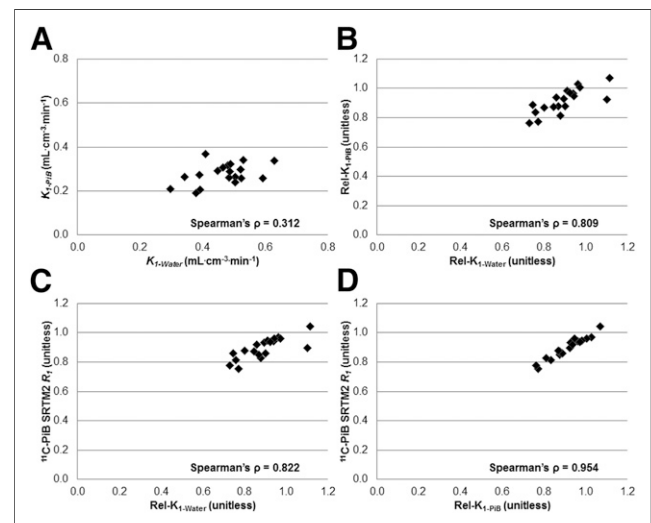


FIGURE 1. Scatterplots for global cortical region (CTX5) depicting relationship between direct delivery ([A] $K_{1\text{-Water}}$ and $K_{1\text{-PiB}}$) and relative delivery ([B] Rel- $K_{1\text{-Water}}$ and Rel- $K_{1\text{-PiB}}$; [C] Rel- $K_{1\text{-Water}}$ and ¹¹C-PiB SRTM2- R_7 ; [D] Rel- $K_{1\text{-PiB}}$ and ¹¹C-PiB SRTM2- R_7), with respective Spearman ρ values. There are different axes ranges for A and B–D.

Comparison of RSD for absolute and relative delivery measures generally revealed lower intersubject variability for relative delivery, including primary cortical regions in which RSD was 4.1%–6.3% lower for Rel- $K_{1\text{-Water}}$ than for $K_{1\text{-Water}}$ and 4.1%–8.6% lower for Rel- $K_{1\text{-PiB}}$ than for $K_{1\text{-PiB}}$. The ^{11}C -PiB SRTM2- R_f RSD was 0.4%–3.8% lower than that for the Rel- $K_{1\text{-PiB}}$.

Figure 1 visually shows the relationship between CTX5 delivery parameters. Figure 2 shows example parametric images of Rel- $K_{1\text{-Water}}$ and ^{11}C -PiB SRTM- R_f and DVR for an AD subject, demonstrating similar regional distribution for Rel- $K_{1\text{-Water}}$ and ^{11}C -PiB SRTM- R_f .

Table 3 lists correlations between ^{15}O -water and ^{11}C -PiB delivery parameters (adjusted for CSF dilution). Correlations between $K_{1\text{-Water}}$ and $K_{1\text{-PiB}}$ were low to moderate ($\rho \approx 0.2\text{--}0.5$) and mostly not significant after Bonferroni adjustment. Stronger correlations ($\rho \approx 0.5\text{--}0.8$) were observed between Rel- $K_{1\text{-Water}}$ and Rel- $K_{1\text{-PiB}}$ (significant for most cortical ROIs after Bonferroni adjustment), with more ROIs showing significant correlation between Rel- $K_{1\text{-Water}}$ and ^{11}C -PiB SRTM2- R_f . Highest correlations ($\rho \approx 0.8\text{--}0.9$, $P < 0.001$) were observed between relative ^{11}C -PiB delivery parameters (Rel- $K_{1\text{-PiB}}$ and ^{11}C -PiB SRTM2- R_f). Correlation between ^{15}O -water and ^{11}C -PiB delivery measures without CSF dilution correction yielded similar results (data not shown).

Delivery and Retention Measures

Table 4 shows mean ^{11}C -PiB retention measures for CTX5 that are consistent with previously described group differences (30). Correlations between delivery parameters and ^{11}C -PiB retention for CTX5 are shown in Table 5, noting lack of significant correlations after Bonferroni adjustment. Full correlation results between delivery parameters and ^{11}C -PiB retention are shown in Supplemental Table 2. Correlations between $K_{1\text{-Water}}$ and ^{11}C -PiB retention (CSF-adjusted) were generally negative and low and lacked statistical significance in primary cortical regions. Similar correlations were present when $K_{1\text{-Water}}$ and ^{11}C -PiB retention were not CSF-adjusted (data not shown). In contrast, statistically significant correlations were evident but variable between ^{11}C -PiB relative delivery and retention, mostly with nonarterial-based retention measures (CER90-DVR, SUVR70, SRTM2-DVR; Supplemental Table 2). ACG was the only primary cortical region that showed significant correlations (after Bonferroni adjustment) between relative ^{11}C -PiB delivery and retention measures ($\rho \approx 0.8\text{--}0.9$, $P < 0.001$). In

contrast, without CSF dilution adjustment, no significant correlations were found between ^{11}C -PiB delivery and retention (after Bonferroni adjustment, data not shown).

DISCUSSION

This study focuses on single-session PET measurements of both quantitative CBF and A β plaque binding in controls, MCI, and AD subjects. The results show statistically significant correlations between relative delivery parameters of ^{15}O -water and ^{11}C -PiB PET (i.e., Rel- $K_{1\text{-PiB}}$ and SRTM2- R_f) and lower trend level correlation between $K_{1\text{-Water}}$ and $K_{1\text{-PiB}}$ for primary cortical regions. Secondly, minimal significant correlations were found between measures of delivery and ^{11}C -PiB retention.

It is well established that the capacity of any radioligand to reflect specific binding is limited if ligand binding is rapid relative to ligand delivery from blood to brain (i.e., $k_3 \gg k_1$ and delivery-limited). This was not the case for ^{11}C -PiB, with early results showing a K_1 of 0.22–0.23 mL·cm $^{-3}$ ·min $^{-1}$ (13), relative to k_3 of 0.04–0.05 min $^{-1}$ (for AD subjects). Early ^{11}C -PiB studies also reported regional bias among semiquantitative binding measures, with an overestimation by SUVR and underestimation by reference-tissue binding measures (relative to arterial-based binding measures) (13). Limitations of SUVR are well established (31), and a ^{11}C -PiB SUVR time-dependency study showed that 40- to 60-min and 50- to 70-min SUVR provided a reasonable compromise between physiologic validity, stability, sensitivity, and clinical feasibility (17). The current study includes data from these published ^{11}C -PiB studies and unpublished paired ^{15}O -water PET studies.

The primary study findings include lack of statistically significant correlations between $K_{1\text{-Water}}$ and $K_{1\text{-PiB}}$ in primary cortical areas, which may partly reflect technical differences including ^{11}C -PiB injection over 20 s that reduces accuracy of $K_{1\text{-PiB}}$ estimation, as compared with $K_{1\text{-Water}}$ determined after rapid ^{15}O -water bolus injection. Even lower correlations were observed between $K_{1\text{-Water}}$ and relative ^{11}C -PiB delivery parameters (data not shown). However, after normalizing both $K_{1\text{-Water}}$ and $K_{1\text{-PiB}}$ to cerebellum, significant positive correlations emerged between Rel- $K_{1\text{-Water}}$ and Rel- $K_{1\text{-PiB}}$ in 4 of 5 primary cortical regions. This positive correlation is not likely driven by CER, as correlation between CER $K_{1\text{-Water}}$ and CER $K_{1\text{-PiB}}$ was not statistically significant ($P = 0.064$) and $K_{1\text{-Water}}$ RSD was similar across ROIs ($\sim 17\%\text{--}20\%$, including CER). These findings may reflect, in part, lower intersubject variability across relative (compared with absolute) delivery measures, as ratios may minimize some variability (e.g., scanner-related measurement variation, variation in intersubject physiologic state). Stronger correlations were observed between Rel- $K_{1\text{-Water}}$ and SRTM2- R_f (than for Rel- $K_{1\text{-PiB}}$), presumably because of greater variance in Rel- $K_{1\text{-PiB}}$ as a calculated ratio of 2 independent parameter estimates, compared with R_f as a single ratio parameter directly estimated by SRTM2. As expected, correlations were strongest between Rel- $K_{1\text{-PiB}}$ and SRTM2- R_f . Overall, these correlations were independent of CSF dilution correction, suggesting robustness against this confound.

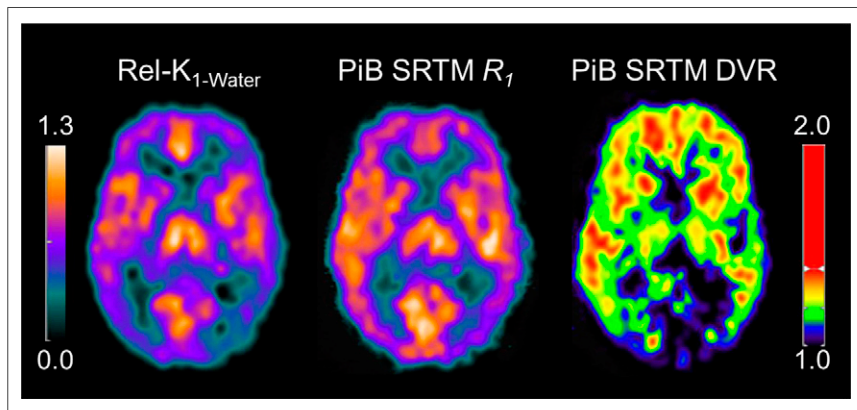


FIGURE 2. Example parametric images of Rel- $K_{1\text{-Water}}$ and ^{11}C -PiB SRTM- R_f and DVR for AD subject (age, 54 y; MMSE, 19) show that Rel- $K_{1\text{-Water}}$ and ^{11}C -PiB SRTM- R_f provide similar distribution of relative flow (images not CSF-corrected).

TABLE 3
Correlation Between ¹⁵O-Water and ¹¹C-PiB Delivery Parameters*†

ROI	Spearman ρ			
	$K_{1\text{-Water}}$ and $K_{1\text{-PiB}}$	Rel- $K_{1\text{-Water}}$ and Rel- $K_{1\text{-PiB}}$	Rel- $K_{1\text{-Water}}$ and ¹¹ C-PiB SRTM2- R_I	Rel- $K_{1\text{-PiB}}$ and ¹¹ C-PiB SRTM2- R_I
ACG	0.311 (0.195)	0.726* (<0.001)*	0.688* (0.001)*	0.984* (<0.001)*
FRC	0.468 (0.043)	0.816* (<0.001)*	0.793* (<0.001)*	0.968* (<0.001)*
LTC	0.422 (0.072)	0.809* (<0.001)*	0.782* (<0.001)*	0.963* (<0.001)*
PAR	0.512 (0.025)	0.628 (0.004)	0.677* (0.001)*	0.967* (<0.001)*
PRC	0.295 (0.221)	0.809* (<0.001)*	0.840* (<0.001)*	0.919* (<0.001)*
CTX5	0.312 (0.193)	0.809* (<0.001)*	0.822* (<0.001)*	0.954* (<0.001)*
MTC	0.234 (0.335)	0.693* (0.001)*	0.784* (<0.001)*	0.901* (<0.001)*
OCC	0.350 (0.141)	0.623 (0.004)	0.707* (0.001)*	0.895* (<0.001)*
OCP	0.486 (0.035)	0.523 (0.019)	0.704* (0.001)*	0.839* (<0.001)*
SMC	0.186 (0.446)	0.689* (0.001)*	0.721* (<0.001)*	0.968* (<0.001)*
AVS	0.509 (0.026)	0.576 (0.010)	0.499 (0.030)	0.839* (<0.001)*
SWM	0.699* (0.001)*	0.613 (0.005)	0.673* (0.002)*	0.902* (<0.001)*
PON	0.247 (0.307)	0.402 (0.088)	0.462 (0.047)	0.921* (<0.001)*
THL	0.225 (0.354)	0.780* (<0.001)*	0.786* (<0.001)*	0.968* (<0.001)*
CER	0.433 (0.064)	NA	NA	NA

*Statistically significant correlations; threshold of $P < 0.0036$ after Bonferroni adjustment.

†Parameters adjusted for CSF dilution.

Data in parentheses are P values.

NA = not applicable.

The secondary findings showed variable significance for regional correlations between delivery (mostly ¹¹C-PiB relative delivery parameters) and ¹¹C-PiB retention that appear to be partly, if not mostly, related to CSF adjustment, as no significant correlations were observed without CSF correction. Correlations between ¹¹C-PiB relative delivery and retention were most notable in ACG, a primary cortical region that exhibits early ¹¹C-PiB deposition and cortical atrophy.

We sought to minimize bias in all kinetic methods but given that SRTM is key to this work, it is important to note potential sources of SRTM bias in its application to ¹¹C-PiB kinetics that are described by 2-tissue compartments (rather than 1 compartment) and that range from specific AD kinetics to nonspecific controls kinetics that may be similar to cerebellum (32). SRTM2 was applied using an average subject-specific SRTM- k_2' constraint determined across ROIs (except CER). We acknowledge that this imperfect estimate of reference tissue clearance rate can bias retention mea-

asures, particularly when time-activity curves in CER and target ROIs are similar (i.e., ¹¹C-PiB-negative), as reported for muscarinic-2 receptor-binding MRTM simulations (33). The k_2' constraints herein were not statistically different between ¹¹C-PiB-positive and ¹¹C-PiB-negative subjects (Mann-Whitney U test $P = 0.278$; cutoffs determined by Cohen, et al. (34)), yielded SRTM2-DVR values that were comparable to other binding measures, and most importantly did not strongly affect R_I that was a primary focus of this work. SRTM- R_I and SRTM2- R_I values were highly correlated (r^2 range, 0.92 [MTC] to 0.99 [CTX5]). Bias in SRTM2- R_I (relative to SRTM- R_I) was less than 10% for primary cortical regions (-3.6% for CTX5), low for PON (1%) and SWM (3.6%), but greater for THL (-8.4%). Yaqub et al. used SRTM as a reference tissue standard for evaluation of simplified voxel-based ¹¹C-PiB analyses (e.g., SUVR, reference Logan, MRTM2 (35), RPM2, SRTM) and reported only a slight difference in quantitative performance across methods, strong correlations across

TABLE 4
CTX5 ¹¹C-PiB Retention Measures

Clinical diagnosis	2T-4k-DVR	ART90-DVR	CER90-DVR	SUVR70	SRTM2-DVR
Controls	1.286 ± 0.267	1.381 ± 0.276	1.310 ± 0.244	1.488 ± 0.345	1.240 ± 0.299
MCI	1.659 ± 0.660	1.781 ± 0.599	1.634 ± 0.565	1.891 ± 0.733	1.645 ± 0.681
AD	1.896 ± 0.582	2.025 ± 0.213	1.997 ± 0.240	2.398 ± 0.334	2.022 ± 0.303

Measures adjusted for CSF dilution.

TABLE 5
Correlation Between Delivery Parameters and ¹¹C-PiB Retention for CTX5^{††}

Parameter	Spearman ρ				
	2T-4k-DVR	ART90-DVR	CER90-DVR	SUVR70	SRTM2-DVR
$K_{1-Water}$	-0.341 (0.196)	-0.281 (0.244)	-0.093 (0.705)	-0.130 (0.596)	-0.093 (0.705)
Rel- $K_{1-Water}$	0.326 (0.217)	0.160 (0.514)	0.202 (0.408)	0.189 (0.437)	0.132 (0.591)
Rel- K_{1-PiB}	0.447 (0.083)	0.426 (0.069)	0.528 (0.020)	0.516 (0.024)	0.533 (0.019)
SRTM2- R_I	0.434 (0.093)	0.385 (0.103)	0.481 (0.037)	0.469 (0.043)	0.489 (0.034)

*Threshold of $P < 0.0036$ for statistically significant correlations after Bonferroni adjustment.

[†]Measures adjusted for CSF dilution.

Data in parentheses are P values.

binding outcomes ($R^2 > 0.95$, except SUVR60–90), best performance by MRTM2 and RPM2, and simulations (6% noise) showing bias in RPM2- BP_{ND} of 0%, SUVR40–60 of 40%, and SUVR60–90 of 50% (14). We do not observe this level of high bias in SUVR using ROI-based analyses with lower noise than voxel-based, using SUVR determined within 40–70 min, and when the reference standard is arterial-based (SUVR50–70 bias 15%) rather than reference-based (SUVR50–70 bias 30%) (17).

The overall findings of this study are consistent with and relevant to findings by others that involved less direct comparisons of delivery. Blomquist et al. reported that changes in PaCO₂ (e.g., from 5.0 to 7.2 kPa) led to changes of similar magnitude in both K_{1-PiB} and CBF ($\approx 50\%$ – 100%) in an anesthetized rhesus monkey, suggesting that K_{1-PiB} may be a useful index of CBF (36). Meyer et al. reported on dual-biomarker imaging of regional A β load and neuronal activity with ¹¹C-PiB using SRTM2 to assess both A β plaque load and relative delivery (19). The high correlations observed herein between Rel- $K_{1-Water}$ and PiB SRTM2- R_I provide direct quantitative evidence that ¹¹C-PiB SRTM2- R_I may be a robust surrogate of regional relative CBF. In addition, ¹¹C-PiB delivery was generally independent of retention, lending further support for determining dual-imaging measures from dynamic ¹¹C-PiB imaging. Lastly, despite flow independence for cross-sectional ¹¹C-PiB retention, a recent report by van Berckel et al. describes how longitudinal ¹¹C-PiB SUVR can be sensitive to longitudinal flow changes (e.g., cortical flow change when reference flow is stable), and this is important to consider and better understand in future studies (20), including those performed with ¹⁸F-labeled A β PET imaging agents (37,38).

CONCLUSION

This study provides quantitative evidence supporting relative ¹¹C-PiB delivery measures as surrogate indices of regional relative CBF. The results also offer further direct evidence that cross-sectional ¹¹C-PiB retention is generally independent of CBF, including SUVR. This study contributes to a body of methodology work that seeks to better understand and define the capabilities of A β PET imaging that is needed to address long-term challenges.

DISCLOSURE

The costs of publication of this article were defrayed in part by the payment of page charges. Therefore, and solely to indicate this fact, this article is hereby marked “advertisement”

in accordance with 18 USC section 1734. Financial support for this work was provided by the NIH (R01AG033042, P50AG005133, R01MH070729, R37AG025516, P01AG025204, K02AG027998), Dana Foundation, and Alzheimer’s Association. William E. Klunk and Chester A. Mathis are coinventors of ¹¹C-PiB, and its license agreement is held between GE Healthcare and University of Pittsburgh. GE Healthcare provided no grant support for this study and had no role in preparing this manuscript. William E. Klunk has served as a consultant to GE Healthcare, Janssen, Pfizer, Lilly, AstraZeneca, Wyeth, Roche, and Elan. Chester A. Mathis has served as a consultant for GE Healthcare, Elan/Wyeth, Novartis, Janssen, Genzyme, Pfizer, Bristol Myers Squibb, IBA, and Baxter Bioscience. Oscar L. Lopez has served as a consultant for Lilly, Lundbeck, Merz, Lilly, and Baxter. Other authors have no conflicts of interest to disclose. No other potential conflict of interest relevant to this article was reported.

ACKNOWLEDGEMENTS

We thank the PET facility staff, particularly Cristy Matan and Christopher Cieply, for technical support. We thank the research volunteers and their families.

REFERENCES

- Cohen AD, Klunk WE. Early detection of Alzheimer’s disease using PiB and FDG PET. *Neurobiol Dis.* 2014;72:117–122.
- Klunk WE, Engler H, Nordberg A, et al. Imaging brain amyloid in Alzheimer’s disease with Pittsburgh compound-B. *Ann Neurol.* 2004;55:306–319.
- Wolk DA, Klunk W. Update on amyloid imaging: from healthy aging to Alzheimer’s disease. *Curr Neurol Neurosci Rep.* 2009;9:345–352.
- Villemagne VL, Pike KE, Chetelat G, et al. Longitudinal assessment of A β and cognition in aging and Alzheimer disease. *Ann Neurol.* 2011;69:181–192.
- Wolk DA, Price JC, Saxton JA, et al. Amyloid imaging in mild cognitive impairment subtypes. *Ann Neurol.* 2009;65:557–568.
- Rowe CC, Ellis KA, Rimajova M, et al. Amyloid imaging results from the Australian Imaging, Biomarkers and Lifestyle (AIBL) study of aging. *Neurobiol Aging.* 2010;31:1275–1283.
- Reiman EM, Chen K, Liu X, et al. Fibrillar amyloid-beta burden in cognitively normal people at 3 levels of genetic risk for Alzheimer’s disease. *Proc Natl Acad Sci USA.* 2009;106:6820–6825.
- Aizenstein HJ, Nebes RD, Saxton JA, et al. Frequent amyloid deposition without significant cognitive impairment among the elderly. *Arch Neurol.* 2008;65:1509–1517.
- Pike KE, Savage G, Villemagne VL, et al. Beta-amyloid imaging and memory in non-demented individuals: evidence for preclinical Alzheimer’s disease. *Brain.* 2007;130:2837–2844.

10. Mintun MA, Larossa GN, Sheline YI, et al. [¹¹C]PIB in a nondemented population: potential antecedent marker of Alzheimer disease. *Neurology*. 2006;67:446–452.
11. Albert MS, DeKosky ST, Dickson D, et al. The diagnosis of mild cognitive impairment due to Alzheimer's disease: recommendations from the National Institute on Aging-Alzheimer's Association workgroups on diagnostic guidelines for Alzheimer's disease. *Alzheimers Dement*. 2011;7:270–279.
12. Tolboom N, Yaqub M, Boellaard R, et al. Test-retest variability of quantitative [¹¹C]PIB studies in Alzheimer's disease. *Eur J Nucl Med Mol Imaging*. 2009;36:1629–1638.
13. Price JC, Klunk WE, Lopresti BJ, et al. Kinetic modeling of amyloid binding in humans using PET imaging and Pittsburgh Compound-B. *J Cereb Blood Flow Metab*. 2005;25:1528–1547.
14. Yaqub M, Tolboom N, Boellaard R, et al. Simplified parametric methods for [¹¹C]PIB studies. *Neuroimage*. 2008;42:76–86.
15. Lopresti BJ, Klunk WE, Mathis CA, et al. Simplified quantification of Pittsburgh compound B amyloid imaging PET studies: a comparative analysis. *J Nucl Med*. 2005;46:1959–1972.
16. Logan J, Alexoff D, Fowler JS. The use of alternative forms of graphical analysis to balance bias and precision in PET images. *J Cereb Blood Flow Metab*. 2011;31:535–546.
17. McNamee RL, Yee SH, Price JC, et al. Consideration of optimal time window for Pittsburgh compound B PET summed uptake measurements. *J Nucl Med*. 2009;50:348–355.
18. Zhou Y, Resnick SM, Ye W, et al. Using a reference tissue model with spatial constraint to quantify [¹¹C]Pittsburgh compound B PET for early diagnosis of Alzheimer's disease. *Neuroimage*. 2007;36:298–312.
19. Meyer PT, Hellwig S, Amtage F, et al. Dual-biomarker imaging of regional cerebral amyloid load and neuronal activity in dementia with PET and ¹¹C-labeled Pittsburgh compound B. *J Nucl Med*. 2011;52:393–400.
20. van Berckel BN, Ossenkoppele R, Tolboom N, et al. Longitudinal amyloid imaging using ¹¹C-PiB: methodologic considerations. *J Nucl Med*. 2013;54:1570–1576.
21. Price JC, Drevets WC, Ruszkiewicz J, et al. Sequential H₂¹⁵O PET studies in baboons: before and after amphetamine. *J Nucl Med*. 2002;43:1090–1100.
22. Minoshima S, Koeppe RA, Mintun MA, et al. Automated detection of the inter-commissural line for stereotactic localization of functional brain images. *J Nucl Med*. 1993;34:322–329.
23. Woods RP, Mazziotta JC, Cherry SR. MRI-PET registration with automated algorithm. *J Comput Assist Tomogr*. 1993;17:536–546.
24. Rosario BL, Weissfeld LA, Laymon CM, et al. Inter-rater reliability of manual and automated region-of-interest delineation for PiB PET. *Neuroimage*. 2011;55:933–941.
25. Marchal G, Rioux P, Petit-Taboue MC, et al. Regional cerebral oxygen consumption, blood flow, and blood volume in healthy human aging. *Arch Neurol*. 1992;49:1013–1020.
26. Raichle ME, Martin WR, Herscovitch P, Mintun MA, Markham J. Brain blood flow measured with intravenous H₂¹⁵O. II. Implementation and validation. *J Nucl Med*. 1983;24:790–798.
27. Innis RB, Cunningham VJ, Delforge J, et al. Consensus nomenclature for in vivo imaging of reversibly binding radioligands. *J Cereb Blood Flow Metab*. 2007;27:1533–1539.
28. Meltzer CC, Kinahan PE, Greer PJ, et al. Comparative evaluation of MR-based partial-volume correction schemes for PET. *J Nucl Med*. 1999;40:2053–2065.
29. Meltzer CC, Zubieta JK, Links JM, Brakeman P, Stumpf MJ, Frost JJ. MR-based correction of brain PET measurements for heterogeneous gray matter radioactivity distribution. *J Cereb Blood Flow Metab*. 1996;16:650–658.
30. Cohen AD, Rabinovici GD, Mathis CA, Jagust WJ, Klunk WE, Ikonomic MD. Using Pittsburgh compound B for in vivo PET imaging of fibrillar amyloid-beta. *Adv Pharmacol*. 2012;64:27–81.
31. Slifstein M. Revisiting an old issue: the discrepancy between tissue ratio-derived binding parameters and kinetic modeling-derived parameters after a bolus of the serotonin transporter radioligand ¹²³I-ADAM. *J Nucl Med*. 2008;49:176–178.
32. Slifstein M, Parsey RV, Laruelle M. Derivation of [¹¹C]WAY-100635 binding parameters with reference tissue models: effect of violations of model assumptions. *Nucl Med Biol*. 2000;27:487–492.
33. Ichise M, Cohen RM, Carson RE. Noninvasive estimation of normalized distribution volume: application to the muscarinic-2 ligand [¹⁸F]FP-TZTP. *J Cereb Blood Flow Metab*. 2008;28:420–430.
34. Cohen AD, Mowrey W, Weissfeld LA, et al. Classification of amyloid-positivity in controls: comparison of visual read and quantitative approaches. *Neuroimage*. 2013;71:207–215.
35. Ichise M, Liow JS, Lu JQ, et al. Linearized reference tissue parametric imaging methods: application to [¹¹C]DASB positron emission tomography studies of the serotonin transporter in human brain. *J Cereb Blood Flow Metab*. 2003;23:1096–1112.
36. Blomquist G, Engler H, Nordberg A, et al. Unidirectional influx and net accumulation of PIB. *Open Neuroimag J*. 2008;2:114–125.
37. Devous MD, Joshi AD, Kennedy I, et al. Employing early uptake data from F18-florbetapir scans as an estimate of regional cerebral blood flow: comparison to F18-FDG. *Alzheimers Dement*. 2014;10(suppl):P102.
38. Joshi A, Pontecorvo M, Navitsky MA, Kennedy IA, Mintun M, Devous MD. Measuring change in beta-amyloid burden over time using florbetapir-PET and a subcortical white matter reference region. *Alzheimers Dement*. 2014;10(suppl):P902.